HAL
open science

Analysis and modelling of entropy modes in a realistic aeronautical gas turbine

Emmanuel Motheau, Yoann Méry, Franck Nicoud, Thierry Poinsot

To cite this version:

Emmanuel Motheau, Yoann Méry, Franck Nicoud, Thierry Poinsot. Analysis and modelling of entropy modes in a realistic aeronautical gas turbine. Journal of Engineering for Gas Turbines and Power, 2013, 135 (9), pp.1-13. 10.1115/1.4024953 . hal-00854160

HAL Id: hal-00854160

https://hal.science/hal-00854160

Submitted on 6 Dec 2021

HAL is a multi-disciplinary open access archive for the deposit and dissemination of scientific research documents, whether they are published or not. The documents may come from teaching and research institutions in France or abroad, or from public or private research centers.

L'archive ouverte pluridisciplinaire **HAL**, est destinée au dépôt et à la diffusion de documents scientifiques de niveau recherche, publiés ou non, émanant des établissements d'enseignement et de recherche français ou étrangers, des laboratoires publics ou privés.

Open Archive TOULOUSE Archive Ouverte (OATAO)
OATAO is an open access repository that collects the work of Toulouse researchers and makes it freely available over the web where possible.

This is an author-deposited version published in : http://oatao.univ-toulouse.fr/
Eprints ID : 9695

To link to this article : DOI:10.1115/1.4024953
URL : http://dx.doi.org/10.1115/1.4024953

To cite this version : Motheau, Emmanuel and Mery, Yoann and Nicoud, Franck and Poinsot, Thierry. *Analysis and modelling of entropy modes in a realistic aeronautical gas turbine.* (2013) Journal Of Engineering For Gas Turbines And Power, vol. 135 (n° 9). pp. 1-13. ISSN 0742-4795

Any correspondance concerning this service should be sent to the repository administrator: staff-oatao@listes-diff.inp-toulouse.fr

Analysis and Modelling of Entropy Modes in a Realistic Aeronautical Gas Turbine

Emmanuel Motheau *
CERFACS - CFD Team
42 av. Gaspard Coriolis
31057 Toulouse - France
Email: emmanuel.motheau@cerfacs.fr

Yoann Mery
Safran Snecma
Rond Point René Ravaud
77550 Moissy Cramayel - France
Email : yoann.mery@snecma.fr

Franck Nicoud
CNRS UMR 5149
University Montpellier II
34095 Montpellier - France
Email : franck.nicoud@univ-montp2.fr

Thierry Poinsot
CNRS - Institut de mécanique des fluides
1 Allée du Professeur Camille Soula
31000 Toulouse - France
Email : thierry.poinsot@cerfacs.fr

ABSTRACT

A combustion instability in a combustor typical of aero-engines is analyzed and modeled thanks to a low order Helmholtz solver. A Dynamic Mode Decomposition (DMD) is first applied to the Large Eddy Simulation (LES) database. The mode with the highest amplitude shares the same frequency of oscillation as the experiment (approx. 350 Hz) and it shows the presence of large entropy spots generated within the combustion chamber and convected down to the exit nozzle. The lowest purely acoustic mode being in the range 650-700 Hz, it is postulated that the instability observed around 350 Hz stems from a mixed entropy/acoustic mode where the acoustic generation associated with the entropy spots being convected throughout the choked nozzle plays a key role. A Delayed Entropy Coupled Boundary Condition is then derived in order to account for this interaction in the framework of a Helmholtz solver where the baseline flow is assumed at rest. When fed with appropriate transfer functions to model the entropy generation and convection from the flame to the exit, the Helmholtz solver proves able to predict the presence of an

*Address all correspondence to this author.

unstable mode around 350 *Hz, in agreement with both the LES and the experiments. This finding supports the idea that the instability observed in the combustor is indeed driven by the entropy/acoustic coupling.*

Nomenclature

p Static pressure
c Sound speed
ω Angular frequency
γ Ratio of the specific heats
q Heat release rate per unit volume
$\hat{g}$ fluctuating part of quantity g
LES Large Eddy Simulations
LEE Linearized Euler Equations
DMD Dynamic Mode Decomposition
DECBC Delayed Entropy Coupled Boundary Condition
T_{res} Flow-through time
ρ Density
J Total stagnation enthalpy
m Mass-flow rate
u Fluid velocity
M Mach number
k Wave number
g_0 Subscript for mean quantity of g
s Entropy
C_p Heat capacity per mass unit at fixed pressure
τ Convection time delay
$\mathbf{n}_{ref}$ Unitary reference vector
$\mathbf{u}_{ref}$ Velocity at reference point
G Gain of the transfer function
Z Impedance
$Z_{p,u}$ Impedance defined with state variables $\hat{p}$ and $\hat{u}$
$Z_{J,m}$ Impedance defined with state variables $\hat{J}$ and $\hat{m}$
Z^0 Impedance imposed at the edge of the zero Mach number domain
Z^M Impedance computed at the edge of the LEE domain

Introduction

It has been long known that combustion instabilities in industrial systems can lead to high amplitude oscillations of all physical quantities (pressure, velocities, temperature, etc.). A classical mechanism for combustion instability is a constructive coupling between acoustic waves and the unsteady combustion that arises when pressure and heat release fluctuations are in phase [1,2]. Another mechanism that may also support self-sustained instabilities relies on the acoustic perturbations induced by entropy spots (temperature and/or mixture heterogeneities say) being generated in the flame region and evacuated through the downstream nozzle [3, 4]. This latter mechanism is particularly relevant to (high speed) reacting flows where the flow through time is small and turbulent mixing cannot significantly reduce the amplitude of the entropy spots being convected from the flame region to combustor exit.

Several recent studies have shown that the Large Eddy Simulation (LES) approach is a powerful tool for studying the dynamics of turbulent flames and their interactions with the acoustic waves [5, 6]. However, these simulations are very CPU demanding and faster tools are required in the design process of new burners. A natural approach is to characterize the

stable/unstable modes in the frequency domain. An approximate linear wave equation for the amplitude $\hat{p}(\mathbf{x})$ of the pressure perturbations $p(\mathbf{x},t) = \hat{p}(\mathbf{x})exp(-j\omega t)$ in reacting flows may be derived from the Navier-Stokes equations [7] and reads:

$$\nabla \cdot \left(c_0^2 \nabla \hat{p}\right) + \omega^2 \hat{p} = j\omega(\gamma - 1)\hat{q} \tag{1}$$

where $\hat{q}(\mathbf{x})$ is the amplitude of the unsteady heat release $q(\mathbf{x},t) = \hat{q}(\mathbf{x})exp(-j\omega t)$, c_0 is the speed of sound, and ω is the complex angular frequency. In order to close the problem, the flame is often modeled as a purely acoustic element thanks to a $n-\tau$ type of model [8] which essentially relates the unsteady heat release to acoustic quantities at reference locations; Eq. (1) then corresponds to a non-linear eigenvalue problem which can be solved by using appropriate algorithms [9].

Eq. (1) relies on the so-called zero Mach number assumption stating that the mean velocity is very small compared to the speed of sound. A recent study suggests that the domain of validity of the zero mean flow assumption might be rather small [10]. One reason for this is that Eq. (1) does not support entropy waves. Thus the acoustic generation due to the entropy spot being accelerated in the nozzle/turbine located downstream of the combustion chamber is not accounted for. Since the production of sound by acceleration of entropy fluctuations is a key phenomenon when dealing with combustion noise [11, 12], neglecting this acoustic source when studying thermoacoustic instabilities is highly questionable. Note also that mixed modes may exist that rely on a convective path and acoustic feedback when the baseline flow is not at rest [3], and that cannot be captured when using Eq. (1).

Nevertheless, this somewhat restrictive assumption is necessary to derive a wave equation for the thermoacoustic perturbations superimposed to a non isentropic baseline flow, the alternative being to use the complete set of Linearized Euler Equations (LEE) [10]. Unfortunately, this would make the computational effort needed to compute the thermoacoustic modes significantly larger (five coupled equations being solved for) than what is required when dealing with Eq. (1). Being able to partly account for the non zero Mach number effects without relying on the LEEs is therefore highly desirable. The objectives of this paper are then as follows:

- analyze fully nonlinear large-eddy simulation data to test for the presence of mixed modes in a realistic combustion chamber;
- develop and validate a methodology to mimic the mean flow effects within the zero Mach number framework (Eq. 1);
- apply the method to a 3D industrial combustor where entropy-acoustic coupling is included in the Helmholtz solver framework.

First, the industrial configuration and associated instability are presented in Section 1; a Dynamic Mode Decomposition (DMD) is applied to the LES results in order to investigate the presence of an entropy-acoustic coupling. A proper formalism is then introduced in Section 2 in order to account for the entropy-acoustic coupling within the zero Mach number framework. The underlying Delayed Entropy Coupled Boundary Condition (DECBC) is also validated in this section by considering an academic quasi-1D combustor mounted on a nozzle. Finally, results from a zero Mach number Helmholtz solver with and without the DECBC approach are presented in Section 3 to illustrate the benefit of the method.

1 Description of the combustor and analysis

1.1 Geometry

The case considered in this study is a combustor developed by the SAFRAN Group for aero-engine applications. The main parts are displayed in Figure 1 which shows the combustion chamber and the casing with primary and dilution holes. The air inlet connected to the upstream compressor is also displayed. Note that the downstream high pressure distributor which connects the combustor to the turbine is modelled by a chocked nozzle with equivalent cross section area. For chocked conditions, this ensures that the chamber sees an acoustic environment close to the actual one. The fuel line is also visible, as well as a cut of the swirled injector used to mix fuel and air and to generate the recirculation zone which stabilizes the flame. In the actual situation, several injectors are mounted all around the azimuthal combustion chamber although only one sector with one injector is displayed in the figure. For confidentiality concerns, some parts of the geometry are not displayed in Figures 1, 2, 3 and 6.

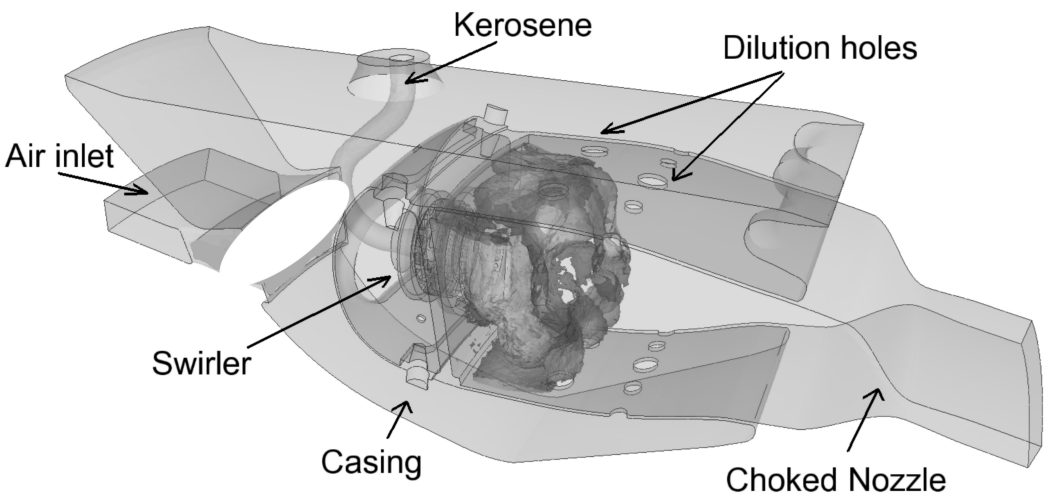

Fig. 1. Description of the configuration of interest. One sector of the azimuthal SAFRAN combustor is represented.

1.2 DMD analysis of the LES data

Experiments were performed by SAFRAN on the configuration described in section 1.1. Under certain operating conditions, the configuration becomes unstable at approximately 350 Hz. To analyze this instability, large eddy simulations (LES) were performed at CERFACS and SAFRAN. For this purpose, the general AVBP [13] code developed at CERFACS and IFP Energies Nouvelles was used. It is based on a cell-vertex formulation and embeds a set of finite element / finite volume schemes for unstructured meshes. In the present study an implementation of the Lax-Wendroff scheme (2nd order in time and space) was retained. Two regimes were computed by LES, corresponding to the two operating conditions investigated experimentally at SAFRAN: one which contains an instability at 350 Hz and one which shows no instability. Although not discussed in this paper, the LES was able to distinguish these two regimes very nicely, displaying a stable turbulent flame for the latter regime and an unstable mode close to 330 Hz for the former. These flows were computed over a 4.5 million elements mesh with the static Smagorinsky subgrid scale model whereas turbulent combustion was represented with the Dynamic Thickened Flame Model [14]. A simple two-step kinetic scheme was used to represent the kerosene-air flame in the combustor [15]. The boundary conditions are imposed through the NSCBC formulation [16] so as to prevent spurious acoustic reflections. Note that as the nozzle is chocked, the physics inside the combustion chamber depends only upon the sonic throat which imposes the effective outlet state. Figure 2 displays a typical snapshot of the LES where the complex 3D flame structure can be seen on top of the temperature field. A pressure signal at a probe within the combustion chamber demonstrates the presence of a thermoacoustic instability at approx. 350 Hz. The amplitude of the limit cycle is quite large and may be explained by the fact that some acoustic dampers such as perforated liners were not included in the computations. However, this result is in the range of pressure fluctuations amplitudes measured in the experiments ($\sim 8.10^4$ Pa peak to peak). Note also the the amplitude was found robust to the shape of the nozzle used to mimic the high pressure distributor.

Dynamic Mode Decomposition (DMD) was applied to the LES data in order to better understand the nature of the instability illustrated in Figure 2. For this purpose, 250 snapshots were recorded over a time range corresponding to approx. 13 cycles characteristics of the instability phenomena, thus leading to a sampling of 20 snapshots by period. This amount of data is sufficient for the DMD to breakdown the reactive turbulent flow into dynamically relevant structures with periodic evolution over time [17]. Note that the input vectors for the DMD algorithm were built from the nodal values of pressure, static temperature and reaction rate at each grid point of the mesh used for the LES. The fluctuating pressure and temperature fields reconstructed from the DMD mode with the highest amplitude are displayed in Figure 3. Note that this mode oscillates at 331 Hz, in good agreement with the experimental data. The four phases displayed in Figure 3 support the idea that the unstable mode of interest relies, at least partly, on an entropy-acoustic coupling. At phase 0, the pressure is low everywhere within the combustion chamber and a pocket of cold gas is present downstream of the primary reaction zone, roughly at

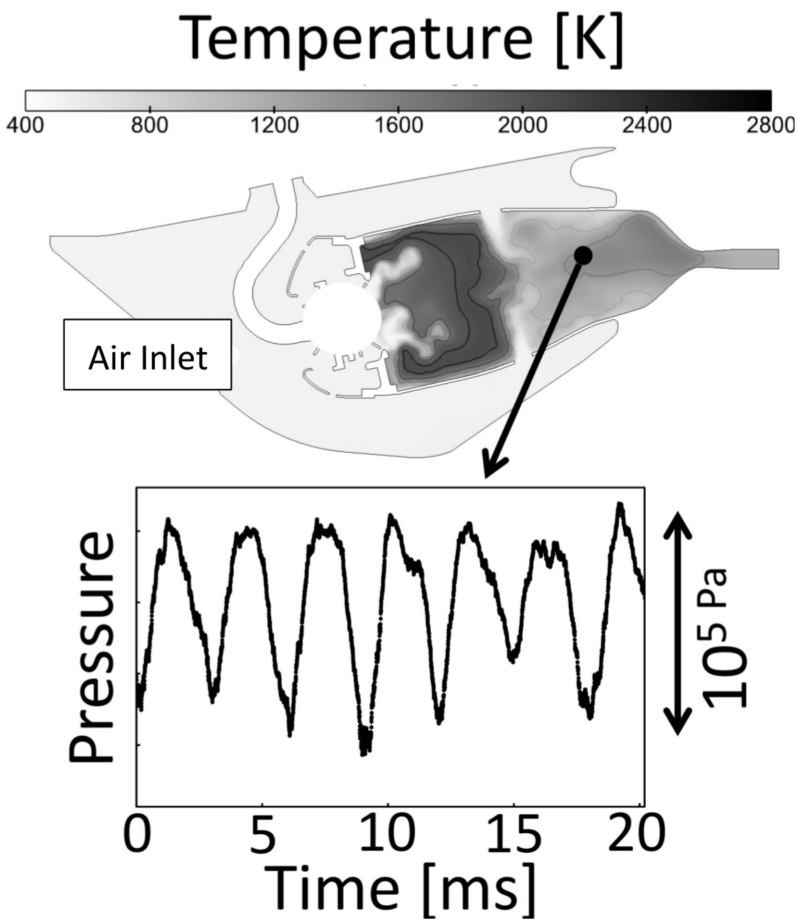

Fig. 2. Typical snapshot from the LES of the SAFRAN combustor and time evolution of pressure within the chamber.

the middle of the combustion chamber. At phase $\pi/2$, this pocket is convected downstream and the unsteady pressure in the chamber is approximately zero. At phase π, this cold pocket interacts with the exit nozzle and a new pocket of hot gas is generated downstream of the primary zone, while the fluctuating pressure within the chamber is now positive. At phase $3\pi/2$, the pocket of hot gas is convected by the mean flow and the pressure within the chamber decreases. Note that each interaction between hot or cold pocket of gas and the nozzle generates acoustics [11] which may propagate downstream (generating what is known as indirect noise) or upstream (generating another perturbation of the flame region and promoting the creation of a new entropy spot).

The idea that the unstable mode close to 350 Hz involves a coupling between entropy and acoustics is further supported by the numerical Helmholtz analysis of the combustor, which shows that the smallest thermoacoustic frequency mode is close to 670 Hz, very far from the observed 350 Hz (see Section 3 for a longer discussion). Although not shown in this paper, the DMD analysis also capture a weaker mode at 680 Hz which only exhibit small pressure fluctuations ($\sim 1.10^3$ Pa) and no significant temperature fluctuations (~ 60 K), suggesting that this mode is purely of acoustic nature, which is consistent with the Helmholtz analysis. In the next two sections, we introduce an acoustic-entropy coupling strategy into the Helmholtz framework to investigate whether such a coupling can predict the 350 Hz mode.

2 Introducing entropy-acoustic coupling in the Helmholtz framework

Since Eq. (1) assumes no mean flow, it is necessary to restrict the study of thermo-acoustic instabilities to only the combustion chamber (where the Mach number is always small). It is then crucial to take into account the proper acoustic environment of the combustor, as for example the presence of a compressor or a turbine; this is illustrated in Figure 4 where Z^0_{up} stands for the proper acoustic impedances that must be imposed at the edges of the Helmholtz domain in order to account for the acoustic waves transmission/reflection due to the compressor and turbine.

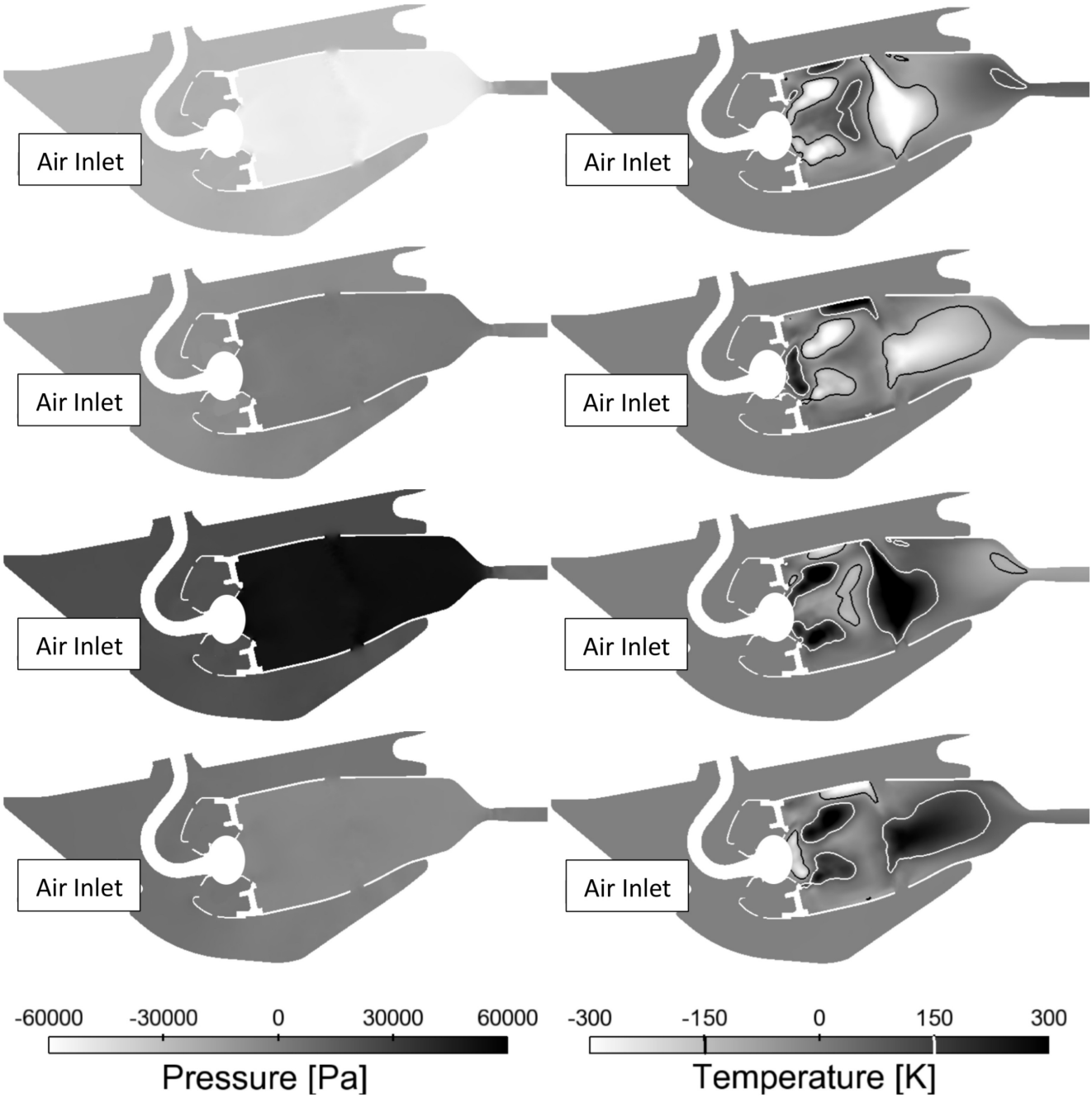

Fig. 3. Fluctuating pressure (left) and temperature (right) from the DMD mode at 331 Hz. From top to bottom, the four rows correspond to phases 0, $\pi/2$, π and $3\pi/2$.

2.1 Acoustic boundary conditions

The acoustic impedance of a non zero Mach number flow element can be assessed analytically under the compact assumption [11]. This acoustic impedance gives rise to a relationship between the inlet acoustic velocity entering the element and the acoustic pressure as follows:

$$\rho_0 c_0 Z_{up}^M \hat{u} - \hat{p} = 0 \quad \text{or alternatively} \quad \frac{c_0}{\rho_0} Z_{mJ}^M \hat{m} - \hat{J} = 0 \tag{2}$$

where $\hat{m}$ and $\hat{J}$ are the (complex amplitude of the) mass flow rate and total enthalpy respectively and Z_{up}^M and Z_{mJ}^M are the impedances associated with variables $(\hat{u}, \hat{p})$ and $(\hat{m}, \hat{J})$ respectively. Moreover, the superscript M denotes the fact that the

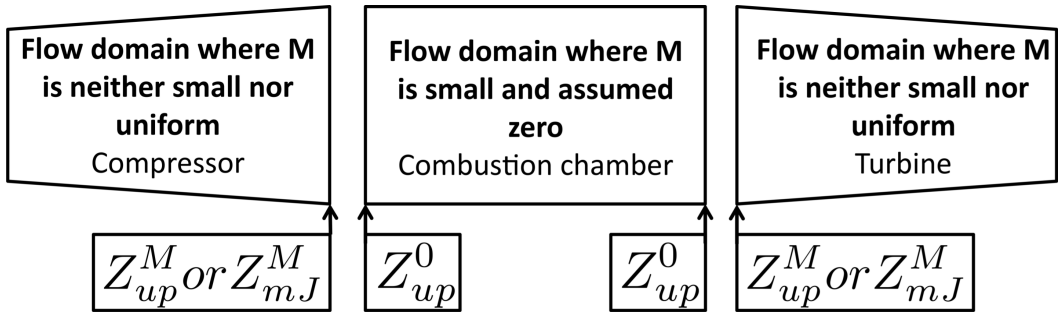

Fig. 4. Schematic view of the modeling strategy: Instead of solving for the LEEs over the whole domain, the Helmholtz equation is solved over the combustion chamber only, the acoustic environment from compressor and turbine being accounted for by imposing proper impedances which take into account the mean flow.

impedances in Eqs. (2) are relevant to acoustic elements where the mean flow is not at rest (as in a compressor or turbine, see Figure 4). Of course, the impedances Z_{up}^M and Z_{mJ}^M are two different complex valued numbers although they represent the same physical element (compressor or turbine). For example, a perfect tube end where the acoustic pressure $\hat{p}$ is zero would correspond to $Z_{up}^M = 0$ but $Z_{mJ}^M = M = u_0/c_0$ because $\hat{J} = \hat{p}/\rho_0 + u_0\hat{u}$ and $\hat{m} = \rho_0\hat{u} + u_0\hat{p}/c_0^2$. More generally, these impedances are related by the following relation:

$$Z_{mJ}^M = (M + Z_{up}^M)/(1 + MZ_{up}^M) \tag{3}$$

Now, since the Helmholtz equation is solved for in the combustion chamber where the mean flow is assumed at rest, a boundary impedance Z_{up}^0 should be imposed in order to account for the effects of the compressor/turbine on the acoustics. Even if $\hat{p}$ is the primary variable (see Eq. (1)) in the combustion chamber, the proper impedance to impose at the edge of the chamber is not necessarily Z_{up}^M. The reason is that the Mach number is zero in the chamber but not when computing Z_{up}^M. A careful analysis of the acoustic flux through the interface between the combustion chamber and the outer acoustic elements [18] shows that a proper choice for Z_{up}^0 is Z_{mJ}^M instead of Z_{up}^M. For example, if a choked feeding line is located upstream of the combustion chamber, the mass flux is constant ($\hat{m} = 0$, $Z_{mJ}^M = \infty$) and the proper boundary condition for the Helmholtz domain is simply $Z_{up}^0 = \infty$. Similarly, if the feeding line imposes the velocity instead of the mass flux ($\hat{u} = 0$, $Z_{mJ}^M = 1/M$, $Z_{up}^M = \infty$), the proper boundary impedance is $Z_{up}^0 = 1/M$ and not ∞.

When the LEEs are solved for everywhere (including the combustion chamber and surrounding elements), entropy fluctuations can be convected to the exit nozzle or turbine where the mean flow is accelerated. These accelerated entropy spots may interact with the acoustics so that the complete boundary condition describing the nozzle or turbine may involve $\hat{s}$, $\hat{u}$ and $\hat{p}$. For example, the relationship derived by [11] for a compact choked nozzle reads:

$$\frac{\hat{u}}{c_0} - \left(\frac{\gamma-1}{2}\right) M \frac{\hat{p}}{\gamma p_0} - \frac{1}{2} M \frac{\hat{s}}{C_p} = 0 \tag{4}$$

or, using the $(\hat{m}, \hat{J})$ variables:

$$\left(\frac{c_0 + (\gamma-1)Mu_0/2}{1-M^2}\right)\hat{m} - \left(\frac{\rho_0 M + (\gamma-1)M\rho_0/2}{1-M^2}\right)\hat{J} - \frac{\rho_0 c_0^2 M}{2C_p}\hat{s} = 0 \tag{5}$$

The third term is usually neglected when assuming zero Mach number in the combustion chamber (because no entropy spot can reach the exit if the convection by the mean flow is neglected) and Eq. (5) allows calculating the impedance Z_{mJ}^M of a

choked compact nozzle. This quantity can then be used as a proper acoustic boundary condition at the edge of the Helmholtz domain; one obtains

$$Z_{up}^{0} = \frac{1}{M}\frac{1+(\gamma-1)M^2/2}{1+(\gamma-1)/2} \tag{6}$$

which is different from the classical nozzle impedance $Z_{up}^{M} = 2/(\gamma-1)M$ derived from Eq. (4).

2.2 Delayed entropy coupled boundary conditions

Imposing the acoustic impedance, Eq. (6), means neglecting the entropy-acoustics coupling and the subsequent sound being generated by the entropy spots flowing through the exit nozzle or turbine. This coupling is contained in the boundary condition Eq. (4) or (5). Note however that $\hat{s}$ is not available in the Helmholtz domain. Thus the entropy fluctuation at the edge of the combustion chamber must be modeled before Eq. (4) or (5) can be applied. Assuming that the entropy fluctuations flowing through the exit have first been generated in the flame region before being convected by the mean flow, one obtains $\hat{s} = \hat{s}_f exp(j\omega\tau_c)$ where $\hat{s}_f$ is the amount of entropy generated by the flame and τ_c is the convection time from the flame to the exit. Consistently with the Helmholtz framework, it is then useful to relate the generated entropy $\hat{s}$ to some acoustic quantity. It is done here in a way similar to the $n-\tau$ model [8] for unsteady heat release, connecting the entropy fluctuation to the acoustic velocity taken at a reference point located upstream of the flame region :

$$\hat{s}_f = G_{\text{us}}\, e^{j\omega\tau_{\text{us}}}\hat{u}_{\text{ref}} \tag{7}$$

where G_{us} and τ_{us} are, respectively, the gain and the time delay of the entropy generation from an acoustic perturbation $\hat{u}_{\text{ref}}$. These quantities can be assessed analytically in the simple case of a 1D premixed flame [18, 19] and read:

$$G_{\text{us}} = -\frac{\rho_u(\gamma-1)(T_b-T_u)C_p^2}{\rho_b u_b c_b^2} \quad ; \quad \tau_{\text{us}} = 0 \tag{8}$$

where the subscripts u and b denote the unburnt and burnt gas respectively. Note that $\tau_{\text{us}} = 0$ because the referential velocity is considered at the flame location. Eventually, for the simple case of a 1D premixed flame in a duct, the proper boundary condition at the downstream edge of the Helmholtz domain is (assuming that burnt gas are present at this boundary and C_p is constant):

$$c_b Z_{up}^{0}\hat{u} - \hat{p}/\rho_b - G_{\text{us}} e^{j\omega\tau_c}\frac{c_b^2(1-M_b^2)}{C_p(\gamma+1)}\hat{u}_{\text{ref}} = 0 \tag{9}$$

Note that $(\rho_b\hat{u},\ \hat{p}/\rho_b)$ replace $(\hat{m},\ \hat{J})$ in Eq. (5) as appropriate in a zero Mach number flow domain. Note also that under the zero Mach number assumption, the momentum equation for the fluctuations reduces to $j\rho\omega\hat{u} = d\hat{p}/dx$ so that Eq. (9) is indeed a boundary condition for the acoustic pressure that can be used when solving the Helmholtz equation.

As a validation case, the Delayed Entropy Coupled Boundary Condition (DECBC) for 1D compact flames, Eq. (9), was used together with the Helmholtz equation to analyze an academic 1D combustor mounted on a compact nozzle (see [18] for the details of the geometry and physical parameters). As illustrated in Figure 5, the proposed coupled boundary condition provides a good prediction of the first acoustic mode in the combustor over the entire range of Mach numbers considered. The first low frequency mode is an entropic mode, also referred to as rumble, which involves the convection of entropy spots from the flame to the exit nozzle; consistently, its frequency of oscillation increases linearly with the Mach number, in contrast to the first acoustic mode whose frequency is virtually constant. Interestingly enough, this low frequency mode is also recovered by the zero Mach number approach completed by the DECBC, demonstrating that the proposed approach properly accounts for the entropy-acoustic coupling in thermoacoustic systems. Of course, when the Helmholtz equation is solved with Eq. (6) as a boundary condition, the entropic mode is not found. Furthermore, the first acoustic mode is not

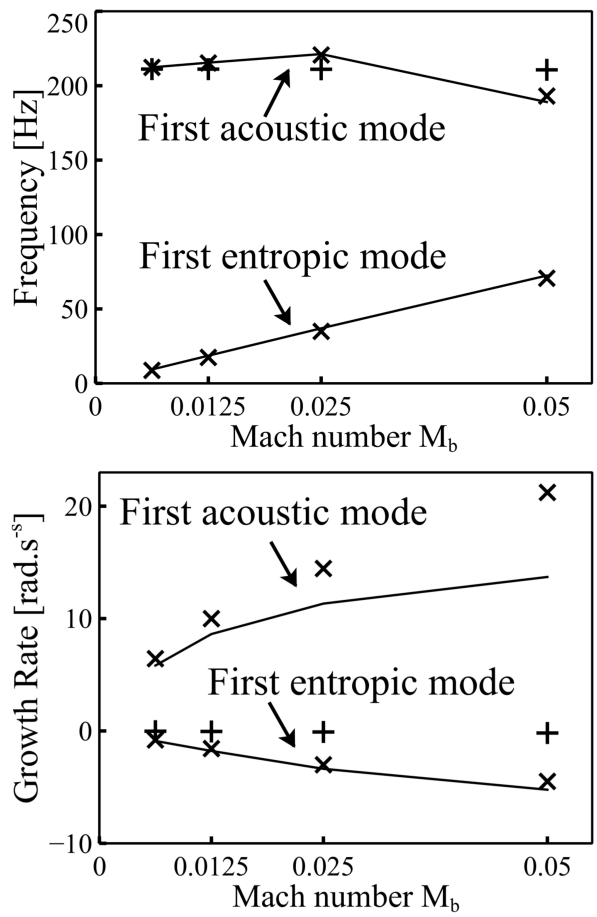

Fig. 5. Frequency of oscillation (upper graph) and growth rate (bottom graph) corresponding to a 1D combustor mounted on a compact choked nozzle. Solid line (——): analytical result at finite Mach number [19]. Symbols: Helmholtz equation at zero Mach number and Eq. (9) as boundary condition, without (+, $G_{\mathrm{us}} = 0$) or with ($\times$, G_{us} from Eq. (8)) entropy coupling.

captured as accurately as when the entropy coupling is modeled at the exit boundary. Even if the comparison is not as good regarding the growth rate of the different modes, the DECBC approach allows a significant improvement of the results from the Helmholtz equation.

3 Helmholtz analysis of the SAFRAN combustor

In this section, Helmholtz analysis of the industrial combustor described in Section 1 is performed. Recall that this configuration exhibits a low frequency mode of oscillation at a frequency significantly smaller than any acoustic mode; it is thus natural to investigate whether the DECBC approach described in Section 2 recovers this low frequency mode.

Name	DECBC	Active Flame	Frequency (Hz)	Growth/decay rate (s^{-1})
Run A	no	no	670	-23
Run B	no	yes	667	-16
Run C	yes	no	320	-68
Run D	yes	yes	320	$+26$

Table 1. Main properties and results of the Helmholtz computations.

Contrary to the simple case considered in Section 2.2, the flame in the SAFRAN combustor is neither 1D nor premixed. Thus, the simple analytical model Eq. (8), used to derived the boundary condition Eq. (9), is not relevant for the 3D case of interest. Instead, the transfer function between the acoustic velocity upstream of the flame and the entropy generated downstream of the primary zone was assessed by post-processing the LES. More precisely, this entropy transfer function was defined as

$$G_{\mathrm{us}}^{\mathrm{LES}} e^{j\omega\tau_{\mathrm{us}}^{\mathrm{LES}}} = \frac{< \hat{s}_f >}{\hat{\mathbf{u}}_{\mathrm{ref}} \cdot \mathbf{n}_{\mathrm{ref}}} \tag{10}$$

where $\mathbf{n}_{\mathrm{ref}}$ is a unitary vector of reference aligned with the main axis of the combustor, $\hat{\mathbf{u}}_{\mathrm{ref}}$ is the acoustic velocity at the reference point depicted in Figure 6 and $< \hat{s}_f >$ is the entropy fluctuation averaged over a small volume located downstream of the primary combustion zone, in agreement with the mode structure observed from the DMD analysis of Section 1.2 (see also Figure 3). Obtaining the acoustic velocity fluctuations $\hat{\mathbf{u}}_{\mathrm{ref}}$ is a difficulty because the reference point is located inside the swirler where hydrodynamics fluctuations occurs. However, as the present study focuses on a low-frequency instability, the hydrodynamic component is considered negligible. Note that this transfer function is similar to but different from the classical flame transfer function which relates the upstream acoustic velocity to the unsteady heat release thanks to a $n-\tau$ type of model [8,9]. Following the rationale developed in section 2.2, the LES data were also used to measure the convection time τ_c^{LES} from the flame region to the end of the combustion chamber (see Figure 6). Note that because the entropy spots decay during their convection through the chamber exit (because of the turbulent mixing and dissipation), the time delay τ_c^{LES} must be completed by a gain G_c^{LES} (smaller than unity) to relate the entropy in the flame region to the entropy at the exit :

$$\hat{s} = G_c^{\mathrm{LES}} e^{j\omega\tau_c^{\mathrm{LES}}} < \hat{s}_f > \tag{11}$$

Finally, the entropy fluctuations in Eq. (5) can be modeled as :

$$\hat{s} = G_{\mathrm{us}}^{\mathrm{LES}} G_c^{\mathrm{LES}} e^{j\omega(\tau_{\mathrm{us}}^{\mathrm{LES}}+\tau_c^{\mathrm{LES}})} \hat{\mathbf{u}}_{\mathrm{ref}} \cdot \mathbf{n}_{\mathrm{ref}} \tag{12}$$

The DECBC condition for the 3D SAFRAN combustor is obtained by injecting Eqs. (6) and (12) into (5) and reads:

$$\begin{aligned} & c_b Z_{up}^0 \hat{\mathbf{u}} \cdot \mathbf{n}_{\mathrm{BC}} - \hat{p}/\rho_b - \\ & G_{\mathrm{us}}^{\mathrm{LES}} G_c^{\mathrm{LES}} e^{j\omega(\tau_{\mathrm{us}}^{\mathrm{LES}}+\tau_c^{\mathrm{LES}})} \frac{c_b^2(1-M_b^2)}{C_p(\gamma+1)} \hat{\mathbf{u}}_{\mathrm{ref}} \cdot \mathbf{n}_{\mathrm{ref}} = 0 \end{aligned} \tag{13}$$

where $\mathbf{n}_{\mathrm{BC}}$ is the unitary outward vector normal to the boundary and ($\rho_b \hat{\mathbf{u}} \cdot \mathbf{n}_{\mathrm{BC}}$, $\hat{p}/\rho_b$) replace ($\hat{m}$, $\hat{J}$) in Eq. (5) as appropriate in a 3D zero Mach number flow domain. The following typical values were obtained from LES and used for the subsequent acoustic analysis: $G_{\mathrm{us}}^{\mathrm{LES}} \approx 160$ m/s/K; $G_c^{\mathrm{LES}} \approx 0.25$; $\tau_{\mathrm{us}}^{\mathrm{LES}} \approx 0.79$ ms; $\tau_c^{\mathrm{LES}} \approx 2.98$ ms. Note that these values were obtained from the first DMD mode at 331 Hz and were supposed independent on frequency.

Several Helmholtz computations were performed by using the AVSP solver developed at CERFACS [9]. In all the cases, a coarse mesh (approx. 10^5 nodes) was generated from the LES grid in order to represent the geometry properly. Additionally, a zero acoustic velocity condition was imposed over all the boundaries except **a)** over the chamber exit where a compact nozzle condition, with or without the DECBC contribution, was imposed and **b)** over the air inlet where the reduced impedance measured with the help of the resulting pressure and velocity fluctuations taken from the DMD mode at 331 Hz was imposed, $Z^{\mathrm{LES}} \approx -2.2 - 1.6i$ (inward). Also, the local speed of sound was deduced from the time averaged LES data and extrapolated on the coarse acoustic mesh.

The main properties of the runs performed are gathered in Table 1 where the frequency of the first mode is also reported. The *Active Flame* column reports whether or not the flame-acoustic coupling (the RHS term of Eq. (1)) is included; if yes,

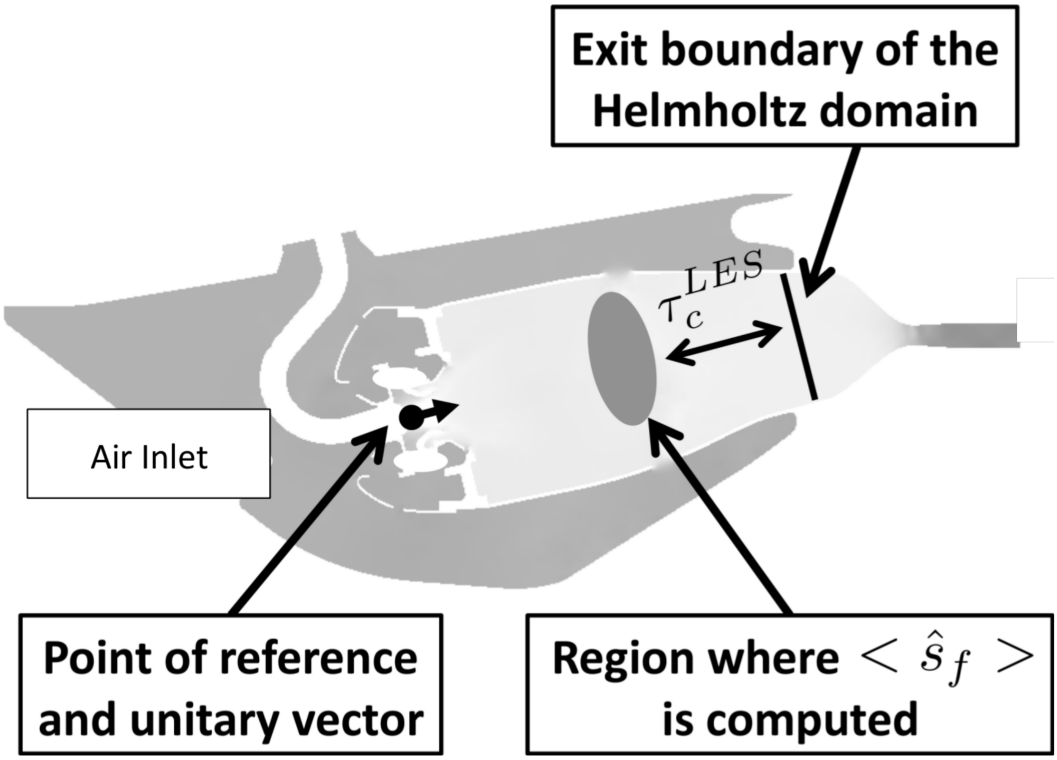

Fig. 6. Computational domain for the Helmholtz analysis. The point of reference and the zone of averaging used for the entropy generation modeling (Eq. 10) are displayed as well as the exit section where the entropy-acoustic boundary condition (Eq. 5) is applied.

the corresponding gain and time delay are computed from the LES in the same way as the entropy-acoustic transfer function. The DECBC column reports the use of the boundary condition (Eq. (13)) developed in this paper. Run A is a classical acoustic computation with variable speed of sound.

As already stated in section 1, the first acoustic mode oscillates at around 670 Hz, very far from the $330-350$ Hz instability observed in the LES and experiment; this acoustic mode is slightly damped (decay rate $-7\ s^{-1}$) due to the acoustic loss at the inlet/outlet. Run B shows that the coupling with the flame does not shift the frequency of oscillation. Introducing the DECBC approach without the flame coupling (Eq. (13) with $G_{\mathrm{us}}^{\mathrm{LES}}$ assessed from LES), Run C produces a mode in the expected frequency range at 320 Hz. This is notably due to the convection delay τ_c^{LES} in Eq. (13) which introduces a longer time scale to the problem. Note however that this mode is damped (decay rate $-68\ s^{-1}$), which is not consistent with this mode being detected in the experiment and LES. Introducing the flame-acoustic coupling together with the DECBC approach corrects this behavior, since Run D gives an unstable mode (growth rate $26\ s^{-1}$) oscillating at 320 Hz, in fair agreement with the LES and experiment. Note that the frequency of oscillation obtained (320 Hz) is rather close to the first DMD mode (331 Hz), thus justifying a posteriori the fact that the transfer function gain and delay were supposed independent on frequency when performing the Helmholtz computations of Table 1.

A limitation of the proposed approach is that the Helmholtz/DECBC solver must be fed by data coming from LES results. This may appear as a strong limitation since the cost of a LES must be paid before the DECBC methodology can be applied. Still, the Helmholtz/DECBC approach remains useful in situations where the same upstream velocity-exit entropy transfer function can be reused for multiple test conditions. Another potential field of application is the study of annular combustors; in this case, one can imagine that a simple one sector LES (containing only one burner) could be performed to feed a Helmholtz/DECBC computation of the whole annular combustor with several identical burners, thus avoiding the extremely CPU demanding LES of the full combustor. This strategy is justified if the flames behave independently and was already used for accounting for the flame response in annular combustors [20, 21].

4 Conclusion

A Delayed Entropy Coupled Boundary Condition was developed as a means to recover some of the convective effects when representing a thermo-acoustic system under the zero Mach number formalism. In this view, a simple model was first used in order to assess the entropy fluctuations at the exit of the combustion chamber. This modeling consists of two steps, one for the entropy generation in the flame region, a second one for the convection/dissipation of the entropy spots through the combustion chamber. This results in a transfer function which relates a reference acoustic velocity in the burner and entropy at the exit of the chamber and which was assessed by post-processing LES data. The acoustics generated by the convection of the entropy spots through the exit nozzle are then treated by applying a proper boundary condition which couples entropy and acoustic quantities. The latter was deduced from the theory of compact nozzles in the present paper. The computation of a SAFRAN combustor which exhibits a low frequency instability demonstrates the potential of the method.

Acknowledgments

E. Motheau gratefully acknowledges support from SNECMA. The authors also thank T. Jaravel and J. Richard (CERFACS) for their technical support for the DMD analysis as well as Y. Méry (SNECMA) for providing the data. Part of this study has been performed during the Summer Program 2012 of the Center for Turbulence Research, Stanford University.

References

[1] Rayleigh, L., 1878. "The explanation of certain acoustic phenomena". *Nature,* **July 18**, pp. 319–321.

[2] Lieuwen, T., and Yang, V., 2005. "Combustion instabilities in gas turbine engines. operational experience, fundamental mechanisms and modeling". In AIAA Prog. in Astronautics and Aeronautics , Vol. 210.

[3] Culick, F. E. C., and Kuentzmann, P., 2006. *Unsteady Motions in Combustion Chambers for Propulsion Systems*. NATO Research and Technology Organization.

[4] Hield, P., Brear, M., and Jin, S., 2009. "Thermoacoustic limit cycles in a premixed laboratory combustor with open and choked exits". *Combust. Flame ,* **156**(9), pp. 1683–1697.

[5] Huang, Y., and Yang, V., 2004. "Bifurcation of flame structure in a lean premixed swirl-stabilized combustor: Transition from stable to unstable flame". *Combust. Flame ,* **136**, pp. 383–389.

[6] Schmitt, P., Poinsot, T., Schuermans, B., and Geigle, K. P., 2007. "Large-eddy simulation and experimental study of heat transfer, nitric oxide emissions and combustion instability in a swirled turbulent high-pressure burner". *J. Fluid Mech. ,* **570**, pp. 17–46.

[7] Poinsot, T., and Veynante, D., 2005. *Theoretical and Numerical Combustion*. R.T. Edwards, 2nd edition.

[8] Crocco, L., 1952. "Aspects of combustion instability in liquid propellant rocket motors. part II.". *J. American Rocket Society ,* **22**, pp. 7–16.

[9] Nicoud, F., Benoit, L., Sensiau, C., and Poinsot, T., 2007. "Acoustic modes in combustors with complex impedances and multidimensional active flames". *AIAA Journal ,* **45**, pp. 426–441.

[10] Nicoud, F., and Wieczorek, K., 2009. "About the zero mach number assumption in the calculation of thermoacoustic instabilities". *Int. J. Spray and Combustion Dynamic,* **1**, pp. 67–112.

[11] Marble, F. E., and Candel, S., 1977. "Acoustic disturbances from gas nonuniformities convected through a nozzle". *J. Sound Vib. ,* **55**, pp. 225–243.

[12] Leyko, M., Nicoud, F., and Poinsot, T., 2009. "Comparison of direct and indirect combustion noise mechanisms in a model combustor". *AIAA Journal ,* **47**(11), pp. 2709–2716.

[13] CERFACS, 2009. *AVBP Handbook - http://cerfacs.fr/∼ avbp/AVBP_V5.X/HANDBOOK*. CERFACS.

[14] Colin, O., Ducros, F., Veynante, D., and Poinsot, T., 2000. "A thickened flame model for large eddy simulations of turbulent premixed combustion". *Phys. Fluids ,* **12**(7), pp. 1843–1863.

[15] Franzelli, B., Riber, E., Sanjosé, M., and Poinsot, T., 2010. "A two-step chemical scheme for Large-Eddy Simulation of kerosene-air flames". *Combust. Flame ,* **157**(7), pp. 1364–1373.

[16] Poinsot, T., and Lele, S., 1992. "Boundary conditions for direct simulations of compressible viscous flows". *J. Comput. Phys. ,* **101**(1), pp. 104–129.

[17] Schmid, P. J., 2010. "Dynamic mode decomposition of numerical and experimental data". *J. Fluid Mech. ,* **656**, pp. 5–28.

[18] Motheau, E., Nicoud, F., and Poinsot, T., 2012. "Using boundary conditions to account for mean flow effects in a zero mach number acoustic solver". *J. Eng. Gas Turb. and Power ,* **134**(11), p. 111502.

[19] Dowling, A. P., 1995. "The calculation of thermoacoustic oscillations". *J. Sound Vib. ,* **180**(4), pp. 557–581.

[20] Wolf, P., Staffelbach, G., Gicquel, L. Y., Müller, J.-D., and Poinsot, T., 2012. "Acoustic and large eddy simulation studies of azimuthal modes in annular combustion chambers". *Combust. Flame ,* **159**(11), pp. 3398 – 3413.

[21] Sensiau, C., Nicoud, F., and Poinsot, T., 2009. "A tool to study azimuthal and spinning modes in annular combustors". *Int. Journal Aeroacoustics,* **8**(1), pp. 57–68.

List of Figures

1 Description of the configuration of interest. One sector of the azimuthal SAFRAN combustor is represented. 4

2 Typical snapshot from the LES of the SAFRAN combustor and time evolution of pressure within the chamber. 5

3 Fluctuating pressure (left) and temperature (right) from the DMD mode at 331 Hz. From top to bottom, the four rows correspond to phases 0, $\pi/2$, π and $3\pi/2$. 6

4 Schematic view of the modeling strategy: Instead of solving for the LEEs over the whole domain, the Helmholtz equation is solved over the combustion chamber only, the acoustic environment from compressor and turbine being accounted for by imposing proper impedances which take into account the mean flow. . . 7

5 Frequency of oscillation (upper graph) and growth rate (bottom graph) corresponding to a 1D combustor mounted on a compact choked nozzle. Solid line (——): analytical result at finite Mach number [19]. Symbols: Helmholtz equation at zero Mach number and Eq. (9) as boundary condition, without ($+$, $G_{\mathrm{us}} = 0$) or with ($\times$, G_{us} from Eq. (8)) entropy coupling. 9

6 Computational domain for the Helmholtz analysis. The point of reference and the zone of averaging used for the entropy generation modeling (Eq. 10) are displayed as well as the exit section where the entropy-acoustic boundary condition (Eq. 5) is applied. 11